Evaluation of flexible flapping wing concept

Thomas Rakotomamonjy[a], Thierry Le Moing[b], Brieuc Danet[c], Xavier Gadoullet[c], Daniel Osmont[d], Marc Dupont[d]

[a]ONERA, Base aérienne 701, 13300 Salon de Provence;
[b]ONERA, 2 av. Édouard Belin, 31055 Toulouse;
[c]ONERA, Chemin de la Hunière, 91761 Palaiseau;
[d]ONERA, 29 av. de la Division Leclerc, 92322 Châtillon

ABSTRACT

ONERA — The French Aerospace Lab — has launched an internal program on biologically-inspired Micro Air Vehicles (MAVs), covering many research topics such as unsteady aerodynamics, actuation, structural dynamics or control. The aim is to better understand the flapping flight performed in nature by insects, and to control state of the art technologies and applications in this field. For that purpose, a flight-dynamics oriented simulation model of a flapping-wing concept has been developed. This model, called OSCAB, features a body and two wings along which the aerodynamics efforts are integrated, so as to determine the global motion of the MAV. The model has been improved by taking into account the flexibility of the wings (flexion of the leading edge and passive torsion of the wings, induced by the flapping motion itself under wing inertia). Thus, it becomes possible to estimate the coupling between flexibility and the aerodynamic forces. Furthermore, the model shows that using elastic properties of the wings allows a diminution of the mechanical energy needed for wings motion, and a reduction of the number of actuators to be implanted into the MAV.

Keywords: micro air vehicles, flapping wings, unstationary aerodynamics, simulation, flexible structures

1. INTRODUCTION

Micro aerial vehicles are defined as small flying autonomous devices, whose wingspan does not exceed 15 cm. Today, they gather a very strong interest in aeronautics, in particular due to promising applications in a wide array of domains, such as monitoring fire risks or vehicle traffic, or serve as "flying googles" operated by a single infantryman for military purposes. Apart from the classical fixed- or rotating-wing MAV concepts mostly developed nowadays, the insect-based, flapping wing flight is an innovative concept, which would allow the capacity to perform mastered hovering flight (as performed in Nature by insects or hummingbirds) as well as quick, short-range maneuvers, while keeping a low-intensity acoustic signature. In the past, many researchers tried to understand and modelize the insect flight, and in particular to explain why the classical aerodynamic mechanisms known by then could not explain the insect flight (the well-known *bumblebees can't fly* paradox). Weis-Fogh was one of the first to demonstrate the existence of unstationary aerodynamic phenomenons, after observing various species of flying insects, and to evaluate the power required for hovering.[1]

Lately, very interesting experimental results were given by Dickinson,[2] who reproduced the flow around a fly wing (*Drosophila melanogaster*) using a scaled wing model flapping in mineral oil (in order to keep the Reynolds number similitude — $Re \approx 10^3$ to 10^4 for insect flight). Three specific aerodynamic effects have been shown up as the cause of a lift gain at low Re : the circulation generated by the rotation of the wing at the end of a stroke, the delayed stall due to the instationarity of the movement, and finally the wake capture, as the wing re-enters the flow it has previously disturbed. Among these conclusions, it has been shown that the phase shift between flapping and rotation movements strongly influences the mean aerodynamic lift.[2]

ONERA conducted between 2002 and 2006 a Federative Research Program: REsearch program on Micro Aerial vehicle and New Technologies Application, or REMANTA,[3] which aimed to develop scientific and technical knowledge in the field of flapping-wing micro air vehicles. As a part of this project, a flight-mechanics, simulation-oriented of a flapping-wing MAV was developed and tested. This model, named *OSCAB* — which stands for *Outil de Simulation de Concept à Ailes Battantes* or "Flapping-wing Concept Simulation Tool" — is based upon a local bidimensional approach: each wing is decomposed into a given number of parallel, chord-length elements,

Health Monitoring of Structural and Biological Systems 2009, edited by Tribikram Kundu,
Proc. of SPIE Vol. 7295, 72951J · © 2009 SPIE · CCC code: 0277-786X/09/$18 · doi: 10.1117/12.816364

and the aerodynamic characteristics (such as velocity and angles of attack) are locally calculated for each element using aerodynamic 2D models. The elementary forces and moments are then summed up and integrated within an inertial frame, in order to obtain the translational and rotational velocities of the global aircraft.

2. AN OVERVIEW OF THE *OSCAB* SIMULATION MODEL

OSCAB simulation model has been developed using a modular structure.[4] At each time step, the values of the internal variables such as velocities, forces and momentums are computed as a function of the controllable inputs. There are three independent inputs for each wing, corresponding to the three possible rotations of the wing with respect to the body : ξ is the angle of the stroke plane ($\xi = 0$ when the wing flaps vertically and $\xi = \pi/2$ when it flaps horizontally), λ is the angle locating the wing within the stroke plane and ν is the angle of rotation of the wing around its longitudinal axis. Since each wing can move independently, there is in the most general case a total of 6 inputs:

$$U = {}^t(\xi_l \ \xi_r \ \lambda_l \ \lambda_r \ \nu_l \ \nu_r). \tag{1}$$

The wing kinematics combined with the global motion of the MAV are used as an input to calculate the local aerodynamic velocities for each wing element. This defines a local aerodynamic frame, and thus a corresponding aerodynamic angle of attack. The elemental forces are then calculated, according to the analytical models adopted to represent the different components of the aerodynamic force, and those forces are summed along the wing, giving a global force and moment applied to the mass center of the MAV.

Finally, the total dynamic components (forces and moments) are integrated within an inertial frame to calculate the kinematic components of the MAV according to Newton's first law (NL) : three translational velocities u, v, w along each axis of the earth-bound inertial frame and three rotational velocities p, q, r (respectively roll, pitch and yaw). An overview of the model structure is given on fig. 1.

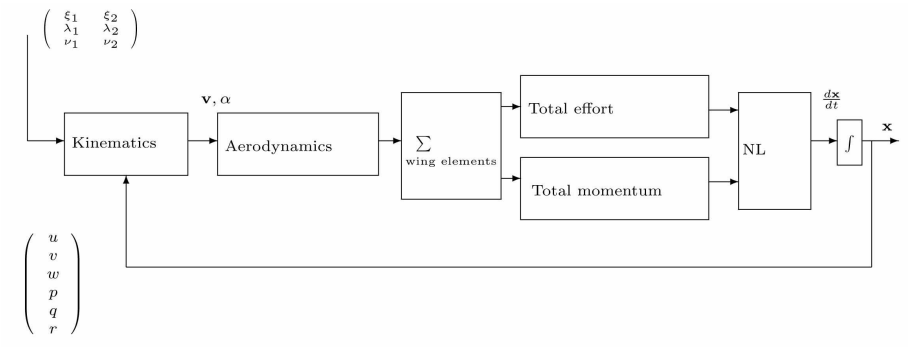

Figure 1. Structure of the simulation model

2.1 Local aerodynamic angle of attack

The frames respectively attached to the ground, the body of the MAV and a given wing (left or right) are respectively denoted as $\mathfrak{R}_n$, $\mathfrak{R}_b$, $\mathfrak{R}_w$. In a first approach, it is supposed that the surrounding air in which flies the MAV is still with respect to the ground frame $\mathfrak{R}_n$, which is equivalent to consider that the wind continuous component in any direction is equal to zero. By considering $F(i)$ the aerodynamic center of the i^{th} wing element, P a fixed point the Galilean frame $\mathcal{R}_0$, G the mass center of the MAV and C the point of articulation of the wing with respect to the body, the local aerodynamic velocity $\vec{V}(i)$ on the considered wing element can be written as:

$$\vec{V}(i) \triangleq \vec{V}_{\text{air}/F(i)} = -\vec{V}_{F(i)/\mathfrak{R}_n} \tag{2a}$$

$$= -\frac{d}{dt}_{/\mathcal{R}_0}(\overrightarrow{PF_i}) \tag{2b}$$

$$= -\frac{d}{dt}_{/\mathcal{R}_0}(\overrightarrow{PO}) - \frac{d}{dt}_{/\mathcal{R}_0}(\overrightarrow{OC}) - \frac{d}{dt}_{/\mathcal{R}_0}(\overrightarrow{CF}(i)) \tag{2c}$$

which gives, after reduction:

$$\vec{V}(i) = -\vec{V}_O - \vec{\Omega}_{nb} \wedge \overrightarrow{OC} - \vec{\Omega}_{bw} \wedge \overrightarrow{CF}(i) - \vec{\Omega}_{nb} \wedge \overrightarrow{CF}(i) \tag{3}$$

where $\vec{V}_O = {}^t(u\ v\ w)$ is the global velocity of the MAV w.r.t. the inertial frame, $\vec{\Omega}_{nb} = {}^t(p\ q\ r)$ the rotation vector between the main body and the inertial frame and $\vec{\Omega}_{bw}$ the rotation vector between the wing and the body (defined using the derivatives of the kinematic angles ξ, λ, ν). By expressing each vector in its reference frame we get:

$$\vec{V} = -\mathbf{B}_{wn}. \begin{pmatrix} u \\ v \\ w \end{pmatrix} - \mathbf{B}_{wb}. \begin{pmatrix} p \\ q \\ r \end{pmatrix} \wedge \left[\mathbf{B}_{wb}. \begin{pmatrix} x_C \\ y_C \\ z_C \end{pmatrix} + \begin{pmatrix} x_F \\ y_F \\ 0 \end{pmatrix} \right] - \vec{\Omega}_{bw} \wedge \begin{pmatrix} x_F \\ y_F \\ 0 \end{pmatrix}. \tag{4}$$

Here $\mathbf{B}_{ij}$ is the 3×3 rotation matrix between $\mathfrak{R}_i$ and $\mathfrak{R}_j$. Then the local aerodynamic angle of attack α_i can be expressed as a function of the components of $\mathbf{v}$ within $\mathfrak{R}_w$:

$$\alpha(i) = \angle(-\vec{V}_x(i) - \mathbf{i}.\vec{V}_z(i)) \qquad (\mathbf{i}^2 = -1) \tag{5}$$

2.2 Aerodynamic forces

For a given wing element, both components (drag and lift) of the stationary aerodynamic forces can be represented within the aerodynamic frame as:

$$\begin{pmatrix} D^{\mathrm{st}} \\ L^{\mathrm{st}} \end{pmatrix} = -\frac{1}{2}\rho S|\vec{V}|^2 \begin{pmatrix} C_x(\alpha) \\ C_z(\alpha) \end{pmatrix} \tag{6}$$

Aerodynamic coefficient functions C_x and C_z are derived from experimental data obtained by Dickinson *et al.*[2,5] The low-Reynolds number specific force components are also taken into account. In particular, it has been shown that the quick rotation of the wing around its main axis at the end of a stroke creates a circulation of the air in the opposite direction, which increases the lift (*rotational circulation*). A model derived from the literature[2,6] expresses this circulation Γ^{rot} as:

$$\Gamma^{\mathrm{rot}} = \pi\dot{\nu}c^2\left(\frac{3}{4} - \frac{x_r}{c}\right) \tag{7}$$

c being the local aerodynamic chord and x_r the distance between the leading edge and the rotation axis.

The unstationary aerodynamic forces also include the added mass effect, which is due to the reaction induced by the acceleration of the fluid mass surrounding the wing. When limiting this phenomenon to translation motion only, this effect can be represented as:[7,8]

$$\Gamma^{\mathrm{mas}} = \frac{\pi}{4}c^2 y_F \frac{1}{|\vec{V}|}\ddot{\lambda} \tag{8}$$

where y_F is the abscissa of the aerodynamic center (defined here as the application point of the aerodynamic forces) of the considered wing element. The resulting elemental force is supposed to act normally to the wing chord, and is obtained from the corresponding circulation *via* :

$$L = \rho|\vec{V}|b\Gamma \tag{9}$$

where b is the width of the considered wing element and $\Gamma = \Gamma^{\mathrm{rot}}$ or Γ^{mas} respectively.

2.3 Forces and moments

The local forces expressed within the wing frame are added, and the dynamic resultant $\vec{R}$ and moment $\vec{M}$ of the aerodynamic forces applied to a given wing (left or right, denoted respectively with l or r subscript) can be obtained:

$$\vec{R}_{l,r} = \sum_{i=1}^{n} \vec{R}_{l,r}(i) \tag{10}$$

$$\vec{M}_{l,r} = \sum_{i=1}^{n} \overrightarrow{GF}(i) \wedge \vec{R}_{l,r}(i) \tag{11}$$

with

$$\vec{R}_{l,r}(i) = \begin{pmatrix} \cos\alpha(i) & -\sin\alpha(i) \\ \sin\alpha(i) & \cos\alpha(i) \end{pmatrix} . \begin{pmatrix} D^{\mathrm{st}}(i) \\ L^{\mathrm{st}}(i) + L^{\mathrm{rot}}(i) + L^{\mathrm{mas}}(i) \end{pmatrix} \tag{12}$$

The aerodynamic forces applied upon the main body of the MAV being neglected, as well as the weight of the wings, the total resultant and moment are respectively equal to:

$$\vec{R} = mg + \mathbf{B}_{nw_l}.\vec{R}_l + \mathbf{B}_{nw_r}.\vec{R}_r \tag{13}$$

$$\vec{M} = \mathbf{B}_{nw_l}.\vec{M}_l + \mathbf{B}_{nw_r}.\vec{M}_r \tag{14}$$

where g is the gravitational acceleration and m the body mass. Newton's second law finally leads to the global translation and rotation velocities, by integration of the global dynamics equations.

3. VALIDATION OF THE SIMULATION MODEL AND IN-LINE OPTIMIZATION OF WING KINEMATICS

3.1 Validation of the aerodynamic model

In order to gain better understanding of the specific, unstationary aerodynamic phenomena at low Reynolds number, experimental tests were carried out in the hydrodynamic tank of ONERA/Lille, with a scaled wing model, flapping in water in order to maintain the Reynolds number similitude.

In parallel of the development of this experimental set-up, a preliminary validation of the simulation model was performed through a comparison with experimental data published by Dickinson.[2] These results, obtained with the Robofly experiment, show a strong influence of the timing of the wing rotation with respect to the flapping upon instantaneous lift. The force measurements of this experiment have been simulated with the OSCAB model using a similar layout: flapping frequency $f = 0.145$ Hz, total wing length $l = 25$ cm, fluid density $\rho = 0.88\text{E}3$ kg.m^{-3}. Wing kinematics were modelled using analytical trigonometric functions chosen to reproduce Robofly inputs and to maintain a constant angle of attack during stroke:

$$\lambda(t) = \lambda_0 \int_0^t \tanh[k_\lambda \cos(\omega u))] du \tag{15}$$

$$\nu(t) = \nu_0 \tanh[(k_\nu \cos(\omega t + \Delta\Phi)] \tag{16}$$

where $\Delta\Phi$ is a phase difference for adjusting timing between flapping and pitch. Simulation results, presented in figure 2, show interesting similarities with Robofly measurements. A phase advance and a phase delay of pitch with respect to flapping generate respectively gain and loss of lift compared with nominal settings. These results prove that this model can reproduce a correct influence of wing kinematics over the global aerodynamic forces.

3.2 In-line optimization of flapping wing kinematics

Onera developed a first experimental set-up, consisting in a rigid, up-scaled wing and a mechanism including a single motor generating limited amplitude motions coupled in flapping and pitch. This experiment was used to reproduce the wing kinematics of forward flapping flight. A linear increase in lift coefficient up to an angle of attack around 20 was observed. The analysis of hovering flight which requires larger amplitude angular motions lead to the conception of a second experimental set-up equipped with two servo-controlled motors for flapping and pitch movements. The first experiments dedicated to the analysis of aerodynamic phenomena at large angle of attack were conducted in 2007 with a rigid flat plate wing. An experimental method for in-line optimization was proposed to search for optimal wing kinematics without requiring preliminary identification of flight dynamics model. A parameter optimization technique with the experimental set-up in the loop was implemented to determine shapes of a periodic wing motion which maximise performance criteria computed from force balance measurements.

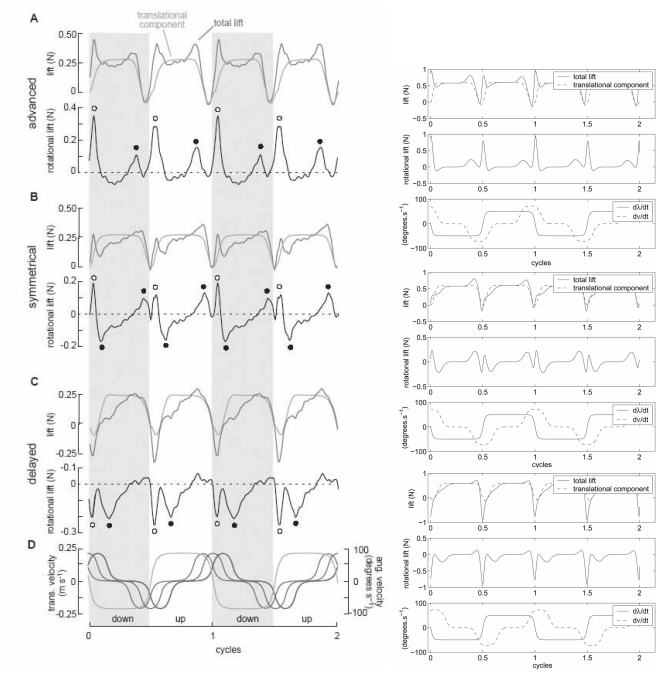

(a) Robofly experimental results (b) OSCAB simulation with similar kinematics

Figure 2. Effect of wing rotation

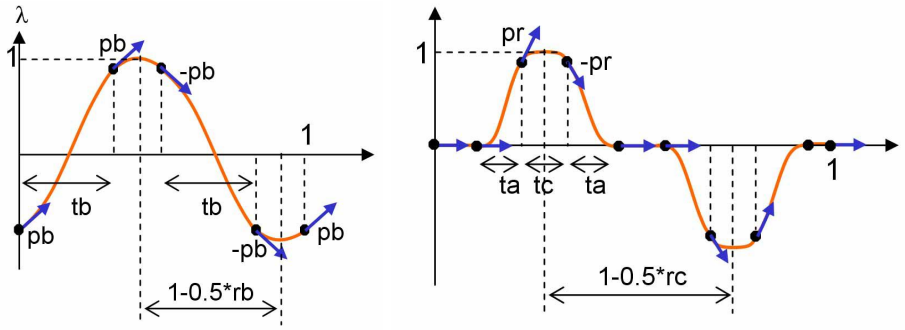

(a) Flapping angle (b) Pitch angle

Figure 3. Flapping and pitch angles modelization (one stroke cycle)

3.3 Parametric Input modelling

The periodic laws representing wing motions have been modelled under a parametric form, chosen to represent various wing kinematics observed in literature review,[9,10] but with a limited number of parameters in order to facilitate the convergence of the optimization algorithm. Flapping model consists in four third-order polynomial arcs. Signal shape is defined by parameters *tb* and *pb* (fig. 3(a)). Duty cycle parameter *rb* can be modified to deliver dissymmetrical signals. Adjustment of one parameter enables the reproduction of periodic functions, continuously varying from square shape to triangle shape as well as cosine function. The pitch wing motion model includes three parameters (fig. 3(b)). Mathematical functions have been derived to reproduce insect wing kinematics which shows nearly constant incidence during stroke.

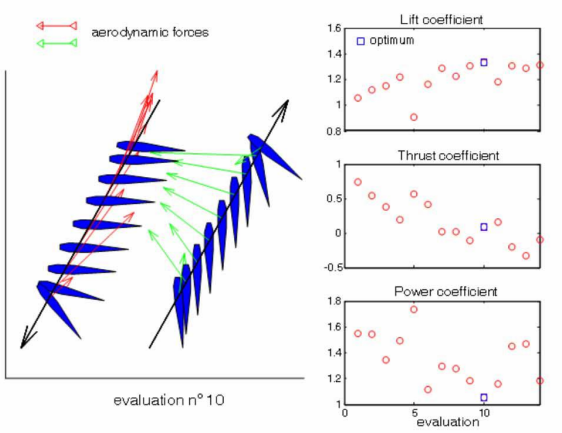

Figure 4. Maximization of mean lift with constraint of zero thrust. Sinusoidal flapping in inclined stroke plane

3.4 Optimization algorithm

A direct search method based on Nelder-Mead algorithm was implemented and used for the optimization. This algorithm, which does not require gradient evaluation, is well-adapted to avoid the effect of measurement noise on finite-difference approximation of gradient. The Nelder-Mead method[11] (which is an extension of the original simplex method proposed by Spendley *et al.*) is based on the comparison of function values at the vertices of a simplex.[12] The algorithm combines three geometric operations (reflection, expansion and contraction) in order to find favourable points. This is a simple, intuitive and relatively stable method which has been used in different areas and cited as a computationally efficient algorithm for the minimization of noisy unconstrained functions.[13] The Nelder-Mead algorithm requires definition of one initial point which was set to the kinematics optimized with the simulation model. Convergence criteria have been introduced to detect simplex degeneracy into a subspace.

The original algorithm was extended to handle bounded parameters and nonlinear inequality constraints. Parameter evolutions are limited by projection every iteration. Constraints are accounted for by an adaptive penalization approach which is a technique robust to the initialization of penalty parameters.

3.5 Results

The first test program was limited to the optimization of a restricted set of parameters in the following configuration:

- Optimization of pitch shape with sinusoidal flapping in horizontal stroke plane to maximize mean lift coefficient;
- Optimization of pitch shape and flapping in horizontal stroke plane to minimize mean power with a mean lift coefficient objective;
- Optimization of pitch with sinusoidal flapping in inclined stroke plane to maximize mean lift coefficient.

The preliminary analysis of these test results shows a fast convergence of the iterative optimization process (fig. 4) and optimal kinematic shapes close to those obtained with the simulation model.

Hydrodynamic force measurements were processed in 2008 with the aim of improving the reliability of the simulation model developed from biographical data, during the REMANTA project. Comparison with simulation results was performed with a simplified aerodynamic model[9] consisting in a single element model, where aerodynamic forces are computed at a specific wing point. Adjustment of lift gradient coefficient and position on wing chord of the reference point used for the estimation of local angle of attack, lead to a good match between instant lift forces over a complete cycle. Figure 5(a) presents contribution of separate components of

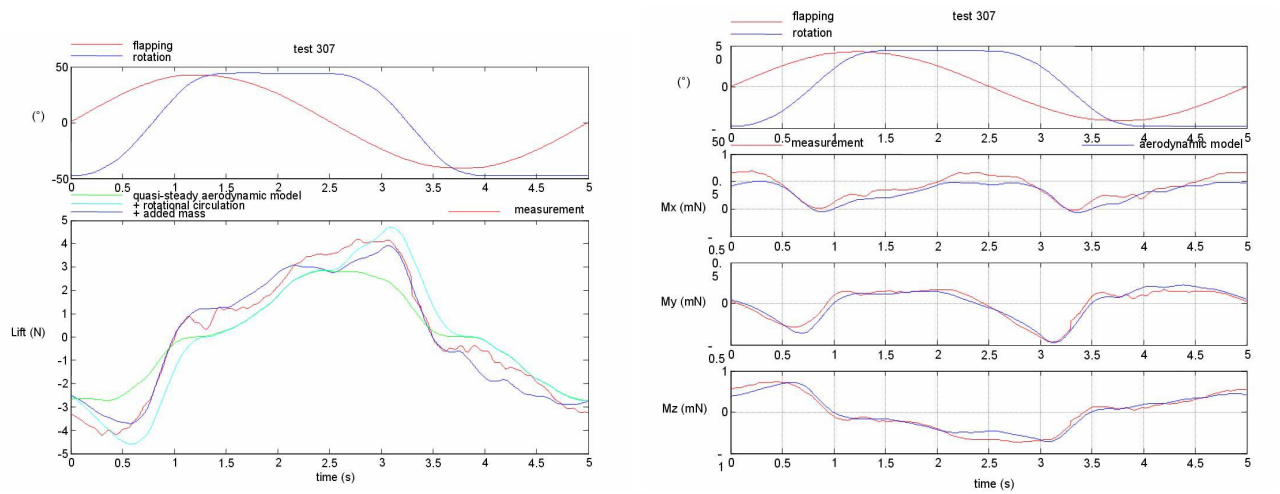

(a) Lift force (b) Moments

Figure 5. Evolution of lift force and moments within a stroke cycle, simulation vs. experimental results

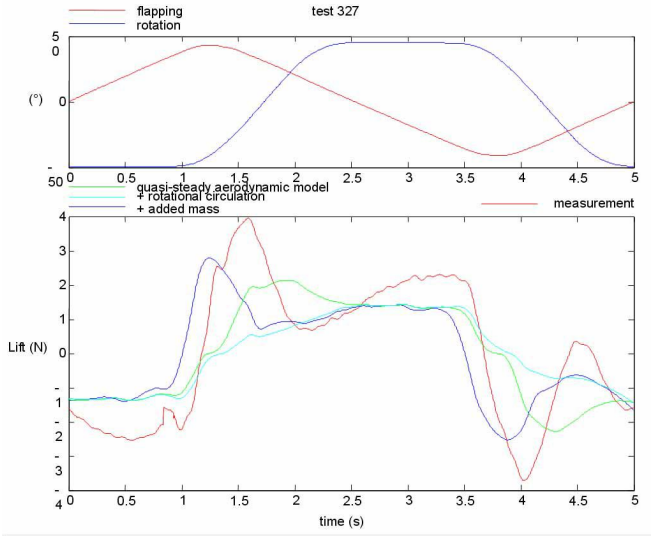

Figure 6. Computational and Experimental forces

the aerodynamic model. Aerodynamic moment model results from global forces applied to the aerodynamic centre. Positioning this point at a distance of 20% of wing chord, in front of the reference point used for the computation of angle of attack, gives a good reproduction of the three moment time histories (fig. 5(b)).

This high level of simulation model fidelity can be verified on most of tests performed during the optimization process. However some wing kinematics characterised by a stroke reversal during pitch motion do not reproduce correct responses with a simple parameter adjustment (fig. 6). The added mass effect seems to induce incorrect phase delay. A more detailed analysis of these data will be conducted more thoroughly to study possible modifications of structure model. Also further experimental tests will be performed to complete the validation of this in-line optimization process with more complex wing kinematics, multi-objective optimization, in hovering and forward flight.

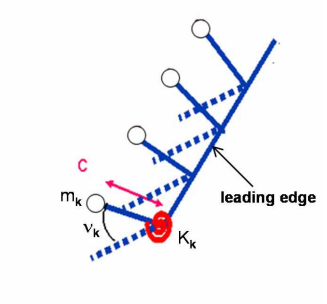

Figure 7. Mechanical representation of the wing

4. WING FLEXIBILITY MODELIZATION

4.1 Relevance of a twisting wing

The optimization of the wing kinematics shows that the rotation of the wing around its longitudinal axis is necessary to generate sufficient aerodynamic forces for the dynamics of the MAV. However, an actuator dedicated to this rotational movement is hard to design and would increase the energy needs. The constraints of mass and size of a MAV lead to find another technological solution. The observation of insects shows that they do not control the angle of the rotation during wing beats. The wing structure may be naturally suited to the movement, and the twisting may result of the inertia of the wing, which undergoes the flapping movement. The mechanical behavior of the wing has been modeled to find out which shape and structure would produce the appropriate torsion. The idea is to find a structure whose resonant frequency is close to the beat frequency. Consequently, the elastic energy stored in the wing would be maximized, with a highly efficient system.

4.2 Modeling of the wing structure

4.2.1 Hypothesis

The two-dimensional approach used in OSCAB to represent the wing has been retained here. Each slice, modeled by a mass m_k concentrated at the trailing edge, is subject to the acceleration of the beat and the reaction of a spring K_k located at the leading edge, which reflects the rigidity of the wing. The torsion of the whole wing then consists in the differential rotation ν_k of the slices (see fig. 7).

The leading edge is not supposed to bend under the solicitation applied at the base of the wing. This hypothesis is confirmed by the observation of insect wings, whose costal vein at the leading edge is much more rigid than others. The bending of the chord is not taken into account either, its influence being slight in the calculus of aerodynamic forces.

4.2.2 Equation, results and discussion

The rotation of each slice, induced by both centrifugal and vertical accelerations of the mass, is described by the harmonic equation (17). All slices are supposed to have the same proper pulsation ω_0, depending on the mechanical characteristics of the whole wing. l_k represents the distance between the slice and the base of the wing, c is as previously the chord length.

$$\ddot{\nu}_k + 2\zeta\omega_0\dot{\nu}_k + \omega_0^2\nu_k = \cos\nu_k\frac{l_k}{c}\ddot{\lambda} + \cos\nu_k\sin\nu_k\dot{\lambda}^2 \tag{17}$$

The flapping angle chosen for the studies suits the triangle shape function described in eq. (15). This will be useful to compare the results between rigid and flexible wings and the analysis will share benefits with the optimizations led on kinematics. The oscillating frequency of flapping is chosen equal to the proper frequency of torsion, so the structure is at resonance. A typical example of the rotational angles obtained for the slices is drawn on figure 8. The maximum value for k is obtained for the farthest slice from the base of the wing. This result is quite logical, given that the value of acceleration is maximum at this point.

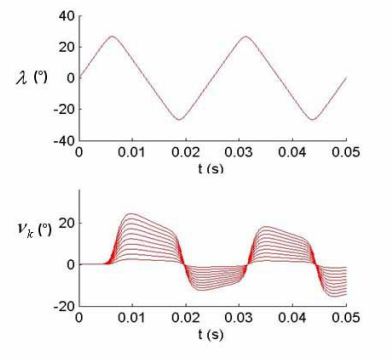

Figure 8. Example of results of rotational angle of slices subject to wing beat

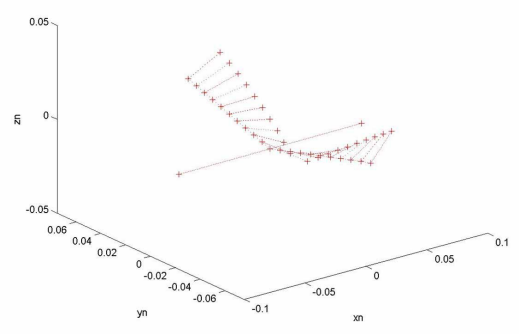

Figure 9. View of the deformation of the wing during the beat

A view of the two flexible wings twisting during the beat is given on figure 9. The mechanical behavior of the structure is similar to the one observed in insects. The value of structural damping ζ is critical, as it strongly influences the level of the torsion angle obtained. However, this factor can only be determined by experimental analysis of the wing. Indeed, it depends on the mechanical properties of the material used, but also on the manufacturing process of the structure. Then, specific characterization has to be led to get a representative value of this important parameter.

4.3 Aerodynamics of flexible wing

The twisting model was then integrated into OSCAB, replacing the pitching angle previously used for the whole wing. The aerodynamic forces were then calculated for each slice, using the classical formulations for stationary and unstationary phenomena. As shown before, the torsion of the wing contributes to the creation of rotational circulation. It is even more important than scale (and therefore the Reynolds number) is low.

Then, it seems necessary to validate the assumption that the structural behavior of the wing is only inertial, as supposed in eq. (17). The comparison between the energy given to the air, the elastic power and the inertial one is quite hard to evaluate. It was then decided to introduce analytic expressions of aerodynamic forces in the oscillatory law for twisting motion, leading to equation (18), where α_k is the local angle of attack; V_{ak} is the local aerodynamic speed.

$$\begin{aligned}(m_k c^2 + K_{maj2})\ddot{\nu}_k + (2\zeta\sqrt{K_k m_k c^2} + K_{rot}V_{ak} + K_{maj1}\cos\alpha_k)\dot{\nu}_k + (K_k - m_k c^2\dot{\lambda}^2)\nu_k \\ = (mcb - K_{maj1}\sin\alpha_k)\ddot{\lambda} - K_{sta1}V_{ak}^2\sin\alpha_k - K_{sta2}V_{ak}^2\sin 3\alpha_k\end{aligned} \tag{18}$$

Both stationary and unstationary forces were taken into account. From an analytical point of view, some of them can be considered as additional terms of structural properties. K_{maj}, which stands for the added mass effect, may influence the value of proper pulsation, whereas K_{rot}, which represents the rotational circulation

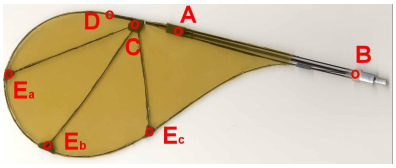

Figure 10. View of the prototype wing

effect, may introduce a term of viscous (aerodynamic) damping. The stationary forces (K_{sta}) only act as additional parts of the leading acceleration. The comparison of values obtained for rotational angles show that the influence of aerodynamics on structure behavior is very small (less than 4%). A slight phase advance was also observed, despite it can't be considered as relevant. These results are consistent with the views expressed in several articles published on the subject.[14] However, the distribution of energy between inertial and fluid dynamic effects strongly depends on the size, mass and stiffness of the wing. This problem of coupling should be considered with caution when changing the scale in the calculus.

5. STRUCTURAL STUDIES

The studies presented above assume that a flexible wing is being flapped and twisted. We are now going to show how we expect to induce these movements. First of all from the work of Combes and Daniel,[15] it is possible to assume that the wing is stiff in bending but with the possibility to be twisted under the inertial forces due to the flapping movement. In order to obtain such a wing, we have realized the following one (see fig. 10): the leading edge A-B of the wing looks like the one of a dragonfly. It is made of three carbon rods figuring the edges of a pyramid with a triangular base (B) the dimension of which is very small (5 mm) with respect to its height (AB = 120 mm). This pyramidal assembly of rods makes the leading edge stiff in flexion and torsion. The rod joining points A and D is stiff. The rod joining points D and B has a smaller diameter than the ones at the leading edge making it possible to obtain its curved shape. The rods CEx, x = a, b, c are used to maintain the curved shape and give some in plane stiffness. A Kapton®film is bonded on the rods adding some additional in plane stiffness and allowing air-coupling. In fact, this structure has been tested in flap and twist on a magnified scale demonstrator using electromagnetic excitation. It appears that this wing has the required bending stiffness and twisting capabilities, but also that the second twisting frequency is of the order of two times the first one which is a great inconvenience. To remedy to this problem a modification is under study to insert in the wing between points A and C a "localized" stiffness making it possible to maintain a high bending stiffness, obtain the desired twisting stiffness and increase the second twisting frequency of the wing to three or four times the first. Then the twisting deformation of the wing under the prescribed flapping movement will be considered as a 1 mode deformation.

In order to induce the flapping movement we have imagine the following structure that we are currently developing. This structure will be called a thorax. The thorax is made, on one side, of a lower U stiff shell stiffened at its upper boundaries and, on the other side, of an upper buckled plate which is hinged in the stiffeners (figs. 11 and 12). In the static state the upper plate is buckled and pre-stressed by the U stiff shell. The flap angle θ is then named α.

If harmonic forces $\pm F(t)$ are applied to the stiffeners normally to the wall of the U shell, the buckled plate moves up and down snapping through the middle surface. The flap angle θ defines the position of the snapping buckled plate. If wings are attached to the plate, these wings follow its snapping through movement and flap up and down. This is the desired result. It has been checked by means of an experiment on a magnified scale demonstrator. The thorax above has been modelized analytically assuming that the upper plate is stiff near the hinges where the wings will be attached and elastic in its middle part. Parametric studies has been made taking into account different elastic middle parts and different static angles α. It appears that there exist a non dimensioned equation satisfied by the flap angle θ which reads for $\theta < \pi/4$, with a very good approximation:

$$\left(\frac{d}{d\tau}\theta(\tau)\right) + 2\Omega\eta\sqrt{k_r}\left(\frac{d}{d\tau}\theta(\tau)\right) + \Omega^2 k_r \sin\theta(\tau)\sigma^2[\theta(\tau)] - \sigma^2(\alpha) - f_a \sin(\Omega r\tau) = 0 \qquad (19)$$

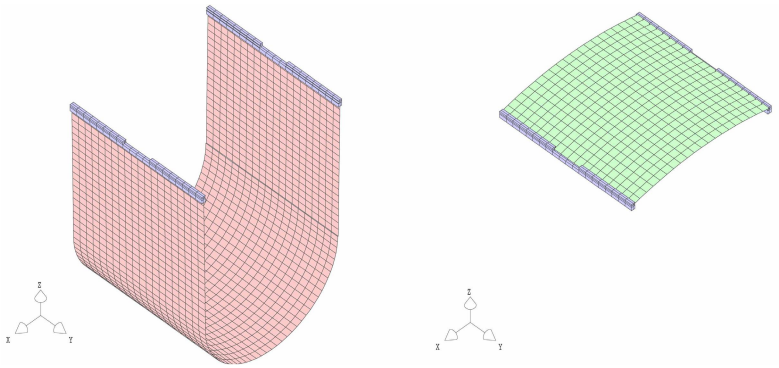

Figure 11. Parts of the thorax structure

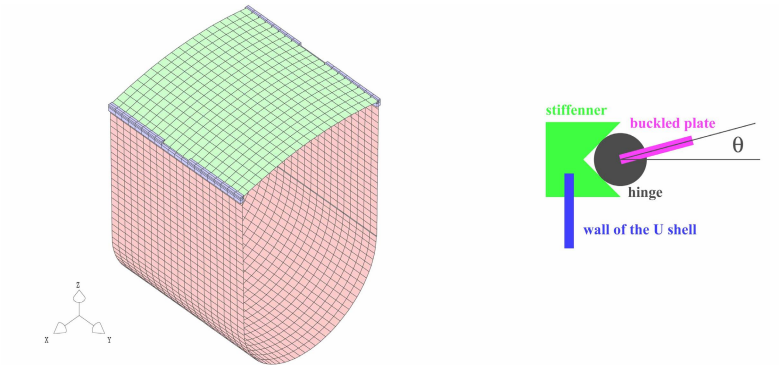

Figure 12. Assembled thorax

where $\Omega = 2\pi$, k_r is a non-dimensional stiffness factor, $\sigma(\theta) = \sin(\theta/2)$, $\tau = t/T(\alpha)$ with $T(\alpha)$ being the period of the small vibrations of the buckled plate in the vicinity of its static state, f_a refers to the amplitude of forces and r is a parameter which is close to 1 and makes it possible to vary the frequency of the flap movement. This means that all the systems have the "same" dynamic behavior governed by this master equation. As an example we show below the stabilized responses of the thorax obtained for a harmonic excitation of the thorax at its natural frequency of vibrations ($r = 1$) for different values of $\alpha = \pi/12$, $\pi/8$, $\pi/6$, $\pi/5$. The responses has been rescaled in amplitude and time but not in phase according to the equation (19).

Figure 13 shows clearly that the dynamics for stabilized flapping does not depend much on the static angle of equilibrium α nor on the elastic properties of the shells as soon as the U shell is stiff enough. This shows that the system proposed is rather robust and that it may be modeled easily by means of a simple equation though it is a nonlinear system.

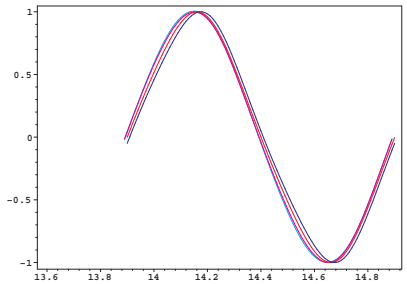

Figure 13. Normalized flap angle $\theta(\tau)/\theta_{\max}(\tau)$ for different values of α

6. CONCLUSION AND PERSPECTIVES

The recent works of ONERA in the domain of flapping-wing micro aerial vehicles have been presented here. First, a simulation model, named *OSCAB*, has been programmmed and validated through comparisons with experimental studies. Then, an experimental set-up has been developed in order to conduct an in-line optimization of the flapping kinematics, using ONERA water tunnel experimental facilities. The flexibility of the wing has also been taken into account, by representing the natural, inertia-induced torsion movement through a discrete repartition of mass along the trailing edge. Concerning the structural studies, the future is to realize a demonstrator with a wing with span of 10 cm, a thorax of width 2.5 cm equipped with electrostrictive films, making it possible to induce in the U-shell of the thorax the harmonic forces required to generate the flapping movement.

REFERENCES

[1] Weis-Fogh, T., "Energetics of hovering flight in hummingbirds and in drosophila," *Journal of Experimental Biology* **56**, 79–104 (1972).

[2] Dickinson, M., Lehmann, F.-O., and Sane, S., "Wing rotation and the aerodynamic basis of insect flight," *Science* **284**, 1954–1960 (June 1999).

[3] Luc-Bouhali, A., "Progress of the remanta project on MAV with flapping wings," in [3^{rd} *International Symposium on Innovative Aerial/Space Flyer Systems*], (Nov. 2006).

[4] Rakotomamonjy, T., Le Moing, T., and Ouladsine, M., "Simulation model of a flapping-wing Micro Air Vehicle," in [*First European Micro Air Vehicle Conference and Flight Competition (EMAV)*], Deutsche Gesellschaft für Ortung und Navigation (July 2004).

[5] Dickinson, M. and Götz, K., "Unsteady aerodynamic performance of model wings at low Reynolds numbers," *Journal of Experimental Biology* **174**, 45–64 (1993).

[6] Norberg, U., [*Vertebrate Flight*], vol. 27 of *Zoophysiology*, Springer-Verlag, Berlin Heidelberg (1990).

[7] Walker, J., "Rotational lift : something different or more of the same ?," *Journal of Experimental Biology* **205**, 3783–3792 (2002).

[8] Fung, Y., [*An introduction to the theory of aeroelasticity*], Dover Publications, New York (1993).

[9] Rakotomamonjy, T., Ouladsine, M., and Le Moing, T., "Modelization and kinematics optimization for a flapping-wing microair vehicle," *Journal of Aircraft* **44**(1), 217–231 (2007).

[10] Bos, F., Lentink, D., van Oudheusden, B., and Bijl, H., "Numerical study of kinematic wing model of hovering insect flight," in [*AIAA Aerospace Sciences Meeting and Exhibit*], (Jan. 2007).

[11] Nelder, J. and Mead, R., "A simplex method for function minimization," *Computer Journal* **7**, 308–313 (1965).

[12] Spendley, W., Hext, G., and Himsworth, F., "Sequential applications of simplex designs in optimization and evolutionary operation," *Technometrics* **4**(4) (1962).

[13] Bortz, D. and Kelley, C. T., "The simplex gradient and noisy optimization problems," in [*Computational Methods in Optimal Design and Control*], Borggaard, J., Burns, J., Cliff, E., and Schreck, S., eds., *Progress in Systems and Control Theory* **24**, 77–90, Birkhäuser, Boston (1998).

[14] Combes, S. and T.L., D., "Flexural wings and fins: bending by inertial or fluid dynamic forces ?," *Integr. Comp. Biol.* **42**, 1044–1049 (2002).

[15] Combes, S. and Daniel, T., "Flexural stiffness in insect wings. I. Scaling and the influence of wing venation," *Journal of Experimental Biology* **206**, 2979–2987 (2003).

[16] Ellington, C., "The aerodynamics of hovering insect flight," *Philosophical transactions of the Royal Society of London. Biological sciences* **305**, 1–181 (Feb. 1984).